Sub-micrometer-thick and low-loss $Ge_{20}Sb_{15}Se_{65}$ rib waveguides for nonlinear optical devices*

LI Jun (李军)**, **CHEN Fen** (陈芬), **SHEN Xiang** (沈祥)**, **DAI Shi-xun** (戴世勋), **XU Tie-feng** (徐铁峰), **and NIE Qiu-hua** (聂秋华)

Laboratory of Infrared Material and Devices, Faculty of Information Science and Engineering, Advanced Technology Research Institute, Ningbo University, Ningbo 315211, China

(Received 8 December 2014; Revised 28 February 2015)

We report the fabrication and optical properties of sub-micrometer-thick $Ge_{20}Sb_{15}Se_{65}$ chalcogenide rib waveguides. The radio-frequency (RF) magnetron sputtering method is used to deposit 0.83 μm-thick films. A protective layer of SU-8 is employed to prevent the attack of the alkaline developer, and CHF_3 is used as the etching plasma for reactive ion etching (RIE). Finally, the resulted rib waveguides with smooth sidewalls and vertical pattern profiles are rendered. The propagation losses for 4 μm-wide waveguides are measured to be 0.7 dB/cm for transverse electric (TE) modes and 0.68 dB/cm for transverse magnetic (TM) modes at 1 550 nm via the cutback method.

Document code: A **Article ID:** 1673-1905(2015)03-0203-4

DOI 10.1007/s11801-015-4231-y

Chalcogenide glasses (ChGs) are emerging as excellent materials to fabricate planar integrated nonlinear optic (NLO) waveguides for ultrafast all-optical signal processing due to their high optical linear and nonlinear refractive indices, low two-photon absorption and negligible free carrier absorption[1-6]. In order to reduce the operating power and the propagation length of NLO waveguides for compact photonic integrated devices, a high nonlinear parameter of $\gamma=2\pi n_2/\lambda A_{\text{eff}}$ is required to offer significant nonlinear enhancements, where A_{eff} is the effective mode area of the waveguide, and n_2 is the nonlinear refractive index. It can be achieved by reducing the waveguide dimension to sub-micrometer level. On the other hand, the materials with higher nonlinear refractive index n_2 can also be applied to reach this goal.

Among various ChGs, a kind of commercially available glass with the nominal composition of $Ge_{20}Sb_{15}Se_{65}$, known as GASIR2, has the good glass-forming ability, and can be easily produced in large-size samples with good control properties[7]. Compared with the binary ChGs compositions, such as As_2S_3, $Ge_{20}Sb_{15}Se_{65}$ has higher nonlinear refractive index (n_2) at 1 550 nm[8], higher glass transition temperatures (T_g) and lower thermal expansion coefficient which provides better resistance to thermal shock[7,9,10]. Furthermore, the replacement of highly toxic element arsenic (As) with antimony (Sb) makes these Ge-Sb-Se glasses more environmentally-compatible compared with other ternary ChGs, such as Ge-As-Se. Therefore, these materials are attractive for the production of compact NLO planar waveguides[11]. Nevertheless, most works on these materials focused on their infrared transparency for infrared optical devices[10]. Recently, these glasses have also attracted much attention due to their great potential for integrated biological and chemical sensors[12,13]. Rib and strip waveguides based on Ge-Sb-Se radio-frequency (RF) sputtered films have been demonstrated[14]. However, the resulted waveguides are rather limited due to their high losses and relatively large waveguide dimensions. To date, there are few reports on the detailed description of waveguide fabrication of these materials, especially for sub-micrometer-sized waveguides in all-optical NLO devices.

In this paper, we report the fabrication and the optical properties of sub-micrometer-thick and low-loss $Ge_{20}Sb_{15}Se_{65}$ rib waveguides. The RF magnetron sputtering method is used to obtain high quality films. A thin protective layer of SU-8 is applied on the $Ge_{20}Sb_{15}Se_{65}$ film to prevent the chemical attack of the alkaline developer. The reactive ion etching (RIE) method with CHF_3 as an etching plasma is used to pattern the rib waveguides. The low propagation losses of the resulted waveguides are determined by the standard cutback method. In addition, the sources of the loss in the waveguides are also discussed.

$Ge_{20}Sb_{15}Se_{65}$ bulk glasses were prepared in our laboratory by conventional melt-quenching method from a

* This work has been supported by the National Natural Science Foundation of China (No.61377061), the Public Project of Zhejiang Province (No.2014C31146), the Young Leaders of the Academic Climbing Project of the Education Department of Zhejiang Province (No.pd2013092), the Natural Science Foundation of Ningbo City (No.2014A610124), the Open Research Fund of the Most Important Specialty "Information and Communication Engineering" of Zhejiang Province (No.XKXL1321), and the Magna Fund sponsored by K. C. Wong in Ningbo University of China.

** E-mails: lijun@nbu.edu.cn; shenxiang@nbu.edu.cn

mixture of Ge, Sb and Se elemental powders with high purity of 99.999% in evacuated quartz ampoules at 10^{-3} Pa. The sealed ampoules containing the mixtures were heated at 900 °C for 12 h in rocking furnaces to ensure the homogenization of the melting. The ampoules were then quenched in cold water, and swiftly moved to a preheated furnace for annealing at 10 °C below T_g for 4 h to minimize the inner tension induced by a quenching step.

0.83 μm-thick $Ge_{20}Sb_{15}Se_{65}$ films were deposited by RF sputtering onto a silicon wafer covered with a 1.5 μm-thick thermal oxide layer which formed the under-cladding layer. The sputtering targets were directly sliced from bulk glass rods into the form of cylinders with thickness of 2 mm and diameter of 80 mm. The deposition was carried out at an operating argon pressure of 0.266 Pa and RF power of 45 W. During the deposition process, the substrate was mounted on a rotatable holder with diameter of 150 mm. The target was loaded into the 3'' magnetron which was mounted with 45° relative to vertical direction and facing upwards with a distance of 100 mm between the target and substrate. The deposition rate of the sputtered films was typically about 7–10 nm/min. The film thickness was measured at different points of the deposited films by a spectroscopic reflectometer (SCI Filmtek 4000), and the deviation was controlled within ±10 nm with good uniformity. The chemical compositions of the bulk glass and the sputtered films were measured by using energy dispersive analysis X-ray spectrometry (EDAX) equipped in Cambridge S-360 scanning electron microscope (SEM), and the results are presented in Tab.1, which shows that the sputtered films present a composition close to the bulk glass with atom percent uncertainty of ±1%.

Tab.1 Chemical compositions of $Ge_{20}Sb_{15}Se_{65}$ bulk glass and sputtered films with atom percent uncertainty of ±1%

Element	Theoretical value (%)	Bulk (%)	Sputtered film (%)
Ge	20	19.09	20.72
Sb	15	15.80	14.71
Se	65	65.11	64.56

$Ge_{20}Sb_{15}Se_{65}$ rib waveguides were fabricated by photolithography and dry-etching. Since most ChG glasses are chemically sensitive to alkaline developers, a thin protective layer of 100 nm-thick SU-8 (SU-8 2, Micro-Chem Corp) film was spin-coated on the $Ge_{20}Sb_{15}Se_{65}$ film to prevent the chemical attack of the developer (AZ MIF-300). We chose SU-8 as a protective layer here due to its excellent coating feature without any pinhole[15]. Moreover, SU-8 is almost transparent at telecommunication wavelengths so that it is not necessary to remove it from the guide surface before cladding formation, and this makes the fabrication process simpler.

Photoresist (positive PR, Clariant AZ MiR 701) patterns were produced on the SU-8/ $Ge_{20}Sb_{15}Se_{65}$ film using I-line contact optical lithography (Karl Suss MA6 mask aligner) followed by wet development. The layers were etched using inductively coupled plasma (ICP) RIE (Plasmalab System 100, Oxford Instruments) with oxygen-based plasma and CHF_3 plasma, respectively. The remaining PR was removed by wet etching with AZ Kwik Strip. Fig.1 shows the scanning electron microscope (SEM, Hitachi S-4500) image of the typical etched waveguide sidewall profile, in which the top layer is SU-8 and the lower layer is the etched $Ge_{20}Sb_{15}Se_{65}$ waveguide sidewall. It is clearly seen that the etched sidewall and surface are smooth. The reduced chemical etching nature by lowering fluorine radical density and the etched surface passivation by enhancing Teflon-like polymer deposition in CHF_3 plasma would be the reason for improved surface and sidewall roughness[16].

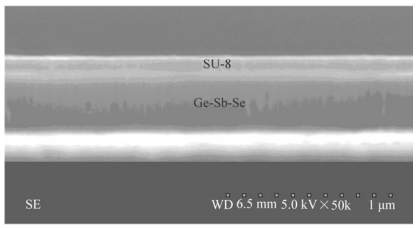

Fig.1 SEM image of the patterned waveguide with smooth etched sidewall and surface

On the other hand, despite of excellent coating feature and simple process of SU-8, the weak adhesion leads to the delamination between SU-8 and inorganic polymer glass (IPG) cladding, so the IPG cladding peeled off from the surface when the wafer was cleaved. In order to promote the adhesion, a thin (2 nm) layer of Al_2O_3 was deposited on SU-8 by atomic layer deposition (ALD) (Savannah, Cambridge NanoTech Inc) after PR stripping. Following ALD, the waveguides were coated with a ~15 μm-thick layer of UV-cured IPG (RPO Pty Ltd) cladding. The end facets were then prepared by hand-cleaving the substrate with a diamond scriber. Fig.2 shows the cross-sectional SEM image of the finished 4 μm-wide waveguides. The finished rib waveguides exhibit nearly vertical pattern profile and have been well defined. The enhanced polymer deposited on the etched sidewall prevents the lateral erosion of the patterns, as a result, the vertical profiles can be obtained. Meanwhile, it is noticeable that the intermediate layer of Al_2O_3 performs well, and we can not see any peeling-off of the cladding in Fig.2.

A tunable laser source (JDS Uniphase SWS16101, 1 510–1 650 nm), a polarization controller, and an InGaAs power meter were used to measure the insertion losses of the waveguides. Due to the small cross section, lensed fibers with mode field diameter of 2.5 μm at $1/e^2$ intensity are used to couple laser light into and out of the waveguides. For the wavelength of 1 550 nm, the inser-

tion losses of the waveguides were measured by the standard cutback method using three different waveguide lengths of 2.2 cm, 4.5 cm and 6.7 cm. Fig.3 presents the raw insertion losses data gathered during the measurement for transverse electric (TE) and transverse magnetic (TM) modes for three different 4 μm-wide waveguides from a single wafer, and linear fitting of the measurement as a function of the waveguide length is also shown. The measurement uncertainty is found to be ±0.1 dB, but the deviation between different samples is slightly large.

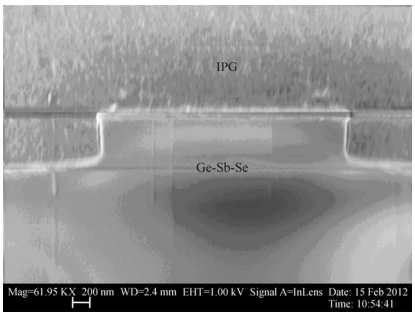

Fig.2 Cross-sectional SEM image of the finished 4 μm-wide rib waveguide

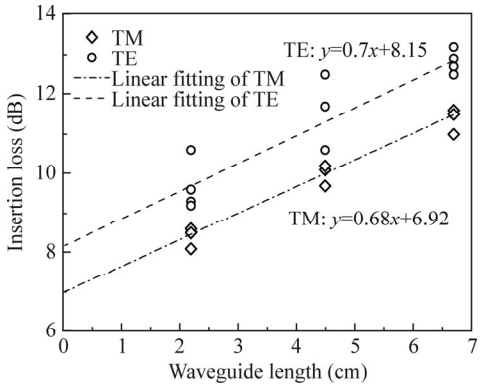

Fig.3 Insertion losses of 4 μm-wide waveguides measured by cutback method

The intercept on the insertion indicates the coupling loss between the guide facet and the lensed fiber calculated by FEMSIM software (RSoft FemSIM^{TM}). From the least squares fitting, the propagation losses at 1 550 nm for 4 μm-wide waveguides are estimated to be about 0.7 dB/cm and 0.68 dB/cm for TE and TM modes, respectively. It should be noted that the TE modes exhibit a little higher losses than the TM modes, since the TE modes are more sensitive to the roughness of the etched sidewalls. However, the difference of the losses between TE and TM modes is insignificant, which indicates that the sidewall roughness from the photolithography and etching processes is not the dominant loss source in these waveguides.

There are two principal scattering loss mechanisms in ChGs, which are the surface scattering arising from the roughness of the interfaces created during the waveguide fabrication process and the Rayleigh scattering from phase separated clusters and inhomogeneities in the deposited films[17]. However, the cutback loss data shown in Fig.3 can not indicate the sources of the losses in the waveguides. To solve this problem, a fiber coupled mercury arc lamp source and an Agilent 86142B optical spectrum analyzer were used to obtain the wavelength dependent propagation loss spectrum over a broad wavelength range from 1 200 nm to 1 700 nm. A typical result is shown in Fig.4, where the dependence of the losses on $1/\lambda^4$ is evident. Note that the small increase in absorption around 1 400 nm and beyond 1 600 nm is due to the overtone absorption from the IPG cladding. It is also significant that the propagation loss around 1 550 nm does not follow the $1/\lambda^2$ dependence as expected for sidewall scattering induced losses[18], but follows the $1/\lambda^4$ dependence induced by Rayleigh scattering. It suggests that the optical loss in these rib waveguides mainly arises from Rayleigh scattering in the thin film itself rather than from the fabrication process, and thus the further improvements on the reduction of the propagation loss can be expected by optimizing the thin film deposition conditions. It is also in agreement with the results of Fig.3 which shows the similar losses for two polarizations and the SEM image in Fig.1 which shows no appreciable sidewall roughness.

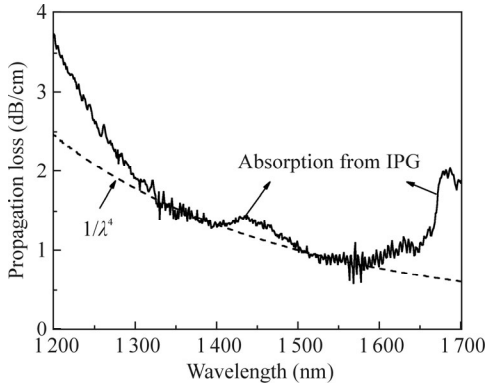

Fig.4 Measured optical propagation loss spectrum of the 4 μm-wide waveguide

In summary, we demonstrate the fabrication of 0.83 μm-thick $Ge_{20}Sb_{15}Se_{65}$ rib waveguides. SU-8 is employed as a protective layer to prevent the attack of alkaline developer and provide excellent coating feature and simple process. CHF_3 with enhanced polymerization tendency is employed in plasma etching process, and not only vertical pattern profile with small etched bias but also smooth etched surface and sidewall are achieved. The resulted waveguides show the propagation losses of 0.7 dB/cm for TE modes and 0.68 dB/cm for TM modes at 1 550 nm, which are demonstrated to be limited mainly by Rayleigh scattering. The excellent properties enable them to be applied as integrated NLO devices for ultrafast all-optical signal processing at telecommunica-

tion wavelengths.

Acknowledgements

Thanks for the support from Centre for Ultra-high-bandwidth Devices for Optical Systems (CUDOS) at Australian National University.

References

[1] Xin Gai, Ting Han, Amrita Prasad, Steve Madden, Duk-Yong Choi, Rongping Wang, Douglas Bulla and Barry Luther-Davies, Optics Express **18**, 26635 (2010).

[2] XU Hui-juan, NIE Qiu-hua, WANG Xun-si, HE Yu-ju, WANG Guo-xiang, DAI Shi-xun, XU Tie-feng, ZHANG Pei-quan, ZHANG Xiang-hua and Bruno Bureau, Journal of Optoelectronics·Laser **24**, 93 (2013). (in Chinese)

[3] HE Yu-ju, WANG Xun-si, NIE Qiu-hua, ZHANG Pei-quan, XU Hui-juan, XU Tie-feng, DAI Shi-xun and ZHANG Pei-qing, Journal of Optoelectronics·Laser **24**, 530 (2013). (in Chinese)

[4] Xu Hui-juan, Wang Xun-si, Nie Qiu-hua, Zhu Min-ming, Jiang Chen, Liao Fang-xing, Zhang Pei-quan, Zhang Pei-qing, Dai Shi-xun, Xu Tie-feng and Tao Guang-ming, Journal of Optoelectronics·Laser **25**, 1109 (2014). (in Chinese)

[5] Benjamin J. Eggleton, Barry Luther-Davies and Kathleen Richardson, Nature Photonics **5**, 141 (2011).

[6] Eggleton B. J., Vo T. D., Pant R., Schröder J., Pelusi M. D., Choi D. Y., Madden S. J. and Luther-Davies B., Laser & Photonics Reviews **6**, 97 (2012).

[7] Zhang X. H., Guimond Y. and Bellec Y., Journal of Non-Crystalline Solids **326**, 519 (2003).

[8] Lenz G., Zimmermann J., Katsufuji T., Lines M. E., Hwang H. Y., Spälter S., Slusher R. E., Cheong S. W., Sanghera J. S. and Aggarwal I. D., Optics Letters **25**, 254 (2000).

[9] Ureña A., Piarristeguy A., Fontana M., Vigreux-Bercovici C., Pradel A. and Arcondo B., Journal of Physics and Chemistry of Solids **68**, 993 (2007).

[10] Nazabal V., Charpentier F., Adam J. L., Nemec P., Lhermite H., Brandily-Anne M. L., Charrier J., Guin J. P. and Moréac A., International Journal of Applied Ceramic Technology **8**, 990 (2011).

[11] Wei W. H., Wang R. P., Shen X., Fang L. and Luther-Davies B., The Journal of Physical Chemistry C **117**, 16571 (2013).

[12] Charrier J., Brandily M. L., Lhermite H., Michel K., Bureau B., Verger F. and Nazabal V., Sensors & Actuators B: Chem **173**, 468 (2012).

[13] Schmidt M. A., Lei D. Y., Wondraczek L., Nazabal V. and Maier S. A., Nature Communications **3**, 1108 (2012).

[14] Zhang W., Dai S., Shen X., Chen Y., Zhao S., Lin C., Zhang L. and Bai J., Materials Letters **98**, 42 (2013).

[15] Choi D. Y., Madden S. J., Bulla D. A., Rode A., Wang R. and Luther-Davies B., Physica Status Solidi C **8**, 3183 (2011).

[16] Choi D. Y., Madden S. J., Rode A., Wang R. and Luther-Davies B., Journal of Applied Physics **104**, 113305 (2008).

[17] Choi D. Y., Madden S. J., Bulla D. A., Wang R., Rode A. and Luther-Davies B., Journal of Applied Physics **107**, 053106 (2010).

[18] Tien P. K., Applied Optics **10**, 2395 (1971).